CHINA FOUNDRY Research & Development
Vol.16 No.2 March 2019
https://doi.org/10.1007/s41230-019-8125-7

Effects of electrode configuration on electroslag remelting process of M2 high-speed steel ingot

Fu-xing Yin [1,2,3], Yu Liang [1], *Zhi-xia Xiao [1,2,3], Jian-hang Feng [1,2,3], Zhi-bin Xie [4], and Yong-wang Mi [4]

1. School of Materials Science and Engineering, Hebei University of Technology, Tianjin 300130, China;

2. Research Institute for Energy Equipment Materials, Hebei University of Technology, Tianjin 300130, China;

3. Tianjin Key Laboratory of Materials Laminating Fabrication and Interfacial Controlling Technology, Tianjin 300130, China;

4. Heye Science and Technology Co., Ltd., Shijiazhuang, Hebei 052165, China

Abstract: The electrode configuration determines the thermophysical field during the electroslag remelting (ESR) process and affects the final microstructure of the ingot. In this work, ingot with a diameter of 400 mm was prepared with two electrode configuration modes of single power ESR process, namely one electrode (OE) and two series-connected electrodes (TSCE). Finite element simulation was employed to calculate the electromagnetic field, flow field and temperature field of the ESR system. The results show that the temperature of the slag pool and the metal pool of the TSCE process is lower and more uniform than that of the OE process. The calculated temperature distribution of the ingot could be indirectly verified from the shape of the metal pool by the experiment. The experimental results show that the depth of the metal pool in the OE ingot is about 160 mm, while the depth of the TSCE ingot is nearly 40 mm shallower than that of the OE ingot. Microstructural comparisons indicate that coarse eutectic carbides are formed in the center of the OE ingot, whereas more even eutectic carbides appear in the center of the TSCE ingot. In general, compared with the OE process, the TSCE process is preferred to remelt high speed steel ingots.

Key words: electroslag remelting; metal pool shape; electromagnetic field; eutectic carbides; high speed steel

CLC numbers: TG142.45 **Document code:** A **Article ID:** 1672-6421(2019)02-126-09

High-speed steels (HSS) are famous for the capacity to retain a high level of hardness even at elevated temperatures caused by cutting metals with a high speed [1-2]. The uniform distribution of fine carbides in the matrix is critical to the HSS performance. However, for the conventional solidification process, eutectic carbides tend to be large and distribute unevenly, especially in industrial-scale ingots. Electroslag remelting (ESR), a suitable process for producing high quality castings, can improve the macrostructure and reduce the non-metallic inclusions, gases and sulfur in steel alloys [3]. Therefore, most of HSS ingots need the ESR process to modify the carbide size and distribution in modern special steel mills.

***Zhi-Xia Xiao**

Female, Senior Engineer. Her research interests mainly focus on the electroslag remelting process, the design and manufacturing of high-performance steels.

E-mail: hbgdxzx@163.com

Received: 2018-09-24; Accepted: 2018-12-18

According to the electrode configuration of a single-power ESR furnace, there are one-electrode (OE) process [4-6], two series-connected electrodes (TSCE) process[7], and three-phase multi-electrode (TPME) process[8-11]. The mode of electrode configuration determines the current circuit. As shown in Fig. 1, the current path of OE process is: transformer → consumable electrode → slag pool → ingot → base plate → transformer, and that of TSCE process is: transformer → one electrode →slag pool →another electrode →transformer. These current circuits can generate different electromagnetic fields, flow fields and temperature fields in the ESR system. Even though the thermophysical field of ESR process could be well simulated by commercial software and preferred process parameters can be obtained [12-15], it is difficult to directly predict the formation of eutectic carbides in HSS ingots due to the complex nucleation and growth [2,16-17]. Therefore, the effects of electrode configuration on eutectic carbides are still unclear.

In this work, single-power ESR experiments were

performed on HSS ingot with a diameter of 400 mm using the OE process and TSCE process, respectively. In order to analyze the effects of electrode configuration, the remelting rate, filling ratio (the ratio of electrode cross-sectional area to mold cross-sectional area) and slag system of the OE process and the TSCE process were guaranteed to be the same. The flow field and temperature field of the slag pool were calculated by ANSYS software. The simulated temperature field of ingot was verified through the experimental shape of the metal pool. Eutectic carbides in the OE ingot and the TSCE ingot were analyzed. Finally, the mode of electrode configuration in the single-power ESR furnace was evaluated.

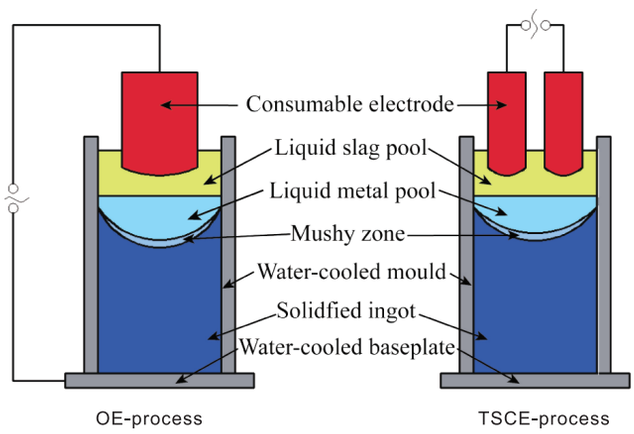

Fig. 1: Schematic diagram of OE process and TSCE process in single-power ESR furnace

1 Experimental procedure

1.1 Experiments

The ESR experiments were carried out in HEYE Special Steel Co., Ltd, China. The slag is composed of 59%CaF_2-19%Al_2O_3-19%CaO-3%SiO_2. In the final stage of the remelting process, some tungsten powder was added in the furnace to trace the shape of the molten steel pool. Then, the OE ingot and TSCE ingot were heat treated at 870 °C for 10 h to avoid cracks and reduce the hardness. After the heat treatment, each ingot was cut into halves, and the shape of the metal pool at the longitudinal section was obtained by metallographic experiments. Samples taken from 50 mm (representing the center structure) and 160 mm (representing the peripheral structure) away from the ingot axis were selected to analyze the microstructure. After being etched using a mixed solution of 30% H_2O_2 100 ml + 42% HF 5 ml, eutectic carbides were observed by an optical microscope and a scanning electron microscope. The volume fraction of eutectic carbides (30 fields in each specimen) was measured using a Zeiss image analyzer.

1.2 Mathematical modeling

Due to the complex coupling between the electromagnetic field, the temperature field and the flow field during the ESR process, it is difficult to accurately redisplay the actual remelting process. Regarding the complex system in the ESR process, the modeling to be described is based on the following assumptions: i) Remelting process is a quasi-steady state; ii) Electrode-slag and slag-metal interfaces are presented by horizontal surfaces; iii) The mold is insulated; iv) Thermophysical properties of the metal and slag are associated only with temperature.

(a) Transport equations for electromagnetic fields

The essential transport equations of electromagnetic fields can be expressed as the following forms:

$$\Delta \times E = \frac{\partial B}{\partial t} \tag{1}$$

$$\Delta \times H = J \tag{2}$$

$$\Delta \cdot B = 0 \tag{3}$$

$$\Delta \cdot J = 0 \tag{4}$$

where, E is the electric field ($V \cdot m^{-1}$); B is the magnetic flux density (T); t is the time (s); H is the magnetic field intensity ($A \cdot m^{-1}$); and J is the current density ($A \cdot m^{-2}$).

The Joule heat ($W \cdot m^{-3}$) and the Lorentz force ($N \cdot m^{-3}$) can be calculated as follows:

$$F_{Lorentz} = J \times B = \mu_0 J \times H \tag{5}$$

$$Q_{Joule} = \frac{J \cdot J}{\sigma} \tag{6}$$

where, μ_0 is the magnetic permeability of free space ($H \cdot m^{-1}$); and σ is the electric conductivity ($\Omega^{-1} \cdot m^{-1}$).

(b) Fluid-flow equations and heat transfer equation

The fluid flow in the slag pool can be explained by the continuity equation and the Navier-Stokes equation as follows:

$$\nabla \cdot \nu = 0 \tag{7}$$

$$\rho\left(\nu \cdot \nabla\right)\nu = -\nabla P + \nabla \cdot \left(\mu_{eff} \cdot \nu\right) + S_S \tag{8}$$

where, ν is the velocity vector of the fluid ($m \cdot s^{-1}$), ρ represents the density ($kg \cdot m^{-3}$), P stands for the pressure force (Pa), μ_{eff} is the effective viscosity (Pa·s), S_S is the source term including electromagnetic force and buoyancy. The turbulent viscosity is calculated by the standard k–ε turbulence model, which has been described in other literature[7]. To simplify the calculation, the fluid flow of the molten metal pool is neglected, and as a compensation, the liquid heat conductivity of the metal is expanded by a factor of 10.

The heat transfer energy equation of the ESR system can be expressed in the following form:

$$\rho C_p \left(V_c \cdot \nabla T\right) = \nabla \cdot k_{eff} \nabla T + S_T \tag{9}$$

where, C_p represents the specific heat ($J \cdot kg^{-1} \cdot K^{-1}$), V_C stands for the remelting rate ($m \cdot s^{-1}$), k_{eff} is the effective thermal conductivity ($W \cdot m^{-1} \cdot K^{-1}$), S_T is the Joule heat generation in slag pool region, or the inner heat source in the metal region ($W \cdot m^{-3}$). The heat transfer between the slag and the falling droplets is negligible, and the surface heat flux is as compensation to the slag/metal interface.

(c) Solution and boundary conditions

The model of two electrode-configuration modes is shown in

Fig. 2(a). The origin of the coordinates is set at the slag/metal interface, and the *Z*-axis is vertical in the ESR system. The model was meshed as shown in Fig. 2(b). Firstly, density of the current and electromagnetic was calculated by the magnetic vector method in ANSYS APDL software. Then the obtained Joule heat and electromagnetic force in slag pool were coupled into ANSYS CFX software to calculate the temperature and flow. The geometrical parameters, operating conditions and physical properties are shown in Table 1.

An air domain, which is cylindrical and has five times the diameter of the ingot, was added to the ESR system to calculate the magnetic field. A flux parallel boundary condition for the magnetic vector potential was applied to the outer surfaces of the air domain. An excitation current load was impressed on the top of one electrode, and the radial current is assumed to be zero. For the OE process, zero electrical potential was set at the bottom of the ingot, while for the TSCE process, zero electrical potential was set in the other electrode. The continuity of the tangential electric field was imposed on the slag/electrode interface and the slag/metal interface.

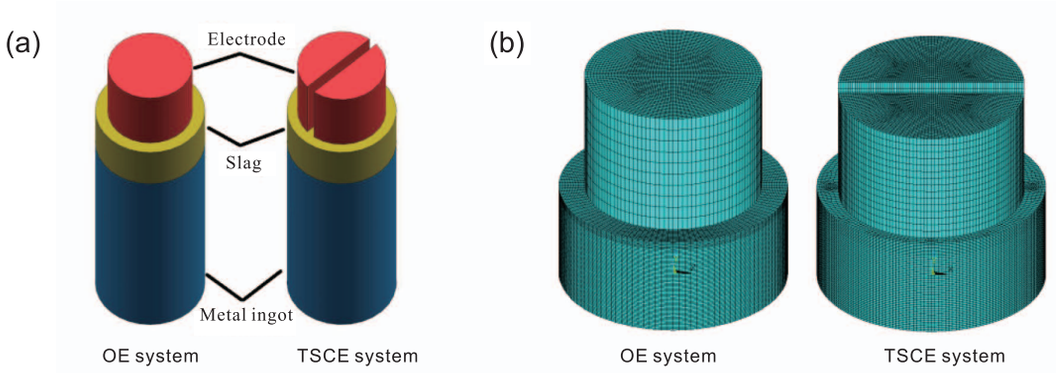

Fig. 2: Schematic of models with two modes of electrode configuration in ESR system (no air domain) (a) and parts of finite element mesh (electrode and slag) (b)

Table 1: Geometrical parameters, operating conditions and physical properties related to ESR process

	Parameter	Value with OE process	Value with TSCE process
Geometry	Ingot (diameter/height), m	0.4/0.8	
	Electrode diameter, m	0.310	
	Mass of slag bath, kg	55	
	Distance of two electrodes, m	-	0.035
Operating conditions	Current amplitude, A	9300	5,200
	Voltage, V	37	44
	Remelting rate by measurement, $kg \cdot min^{-1}$	5	
	Temperature drop of cooling water, K	10	7
Physical properties of metal	Thermal conductivity, $W \cdot m^{-1} \cdot K^{-1}$	31	
	Density, $kg \cdot m^{-3}$	7,500	
	Specific heat, $J \cdot kg^{-1} \cdot K^{-1}$	859	
	Latent heat of fusion, $kJ \cdot kg^{-1}$	211	
	Liquidus/solidus, K	1,688/1,513	
	Electric conductivity, $\Omega^{-1} \cdot m^{-1}$	6.01×10^6	
	Magnetic permeability, $H \cdot m^{-1}$	1.257×10^{-6}	
Physical properties of slag	Thermal conductivity, $W \cdot m^{-1} \cdot K^{-1}$	10.45	
	Density, $kg \cdot m^{-3}$	2,580	
	Specific heat, $J \cdot kg^{-1} \cdot K^{-1}$	1,300	
	Electric conductivity, $\Omega^{-1} \cdot m^{-1}$	234	
	Magnetic permeability, $H \cdot m^{-1}$	1.257×10^{-6}	

A no-slip condition was applied on the liquid/solid interface, and the free surface of the slag pool was set as free slip interface. Although the heat transfer is complicated at the boundary, simplified heat transfer coefficients could be applied on the interfaces of the slag/ingot, the ingot bottom/mold, and the ingot lateral surface/mold. Natural convection as well as thermal radiation were considered on the free surface of the slag pool, and a curve of heat transfer coefficients as a function of temperature was selected. The liquidus temperatures of the slag and the electrode were added on the slag/mold and electrode/slag interfaces, respectively. Determination of these parameters can be found in other literature [7].

2 Results and discussion

2.1 Electromagnetic field of electrode and slag

Figure 3 shows the calculated electric potential, current density and Joule heat generation in the main vertical section of electrode and slag zone. For the OE process, electric current flows from the electrode through the slag pool, and finally into the ingot, as shown in Fig. 3(b). The electric potential gradient around the end of the electrode is great (Fig. 3a). Therefore, the slag pool region around the edge of the electrode has the highest current density with a maximum of about 3.65e5 A·m^{-2} (Fig. 3b). Joule heat generation in the slag region is concentrated below the end of the electrode. The region where Joule heat is greater than 18 MW·m^{-3} appears as a pot-bottom shape shown in Fig.3(c), which can cause high temperatures. Far from the end of the electrode, the current density of the slag pool is low. The upper part of the slag pool has the lowest current density. Therefore, Joule heat drops sharply from the electrode/slag interface to the slag/metal interface along the axial direction, and from the center of the slag pool to the periphery along the radial direction.

For the TSCE process, electric current flows mainly from one electrode through the slag bath into the other as seen in Fig. 3(e). The region of the maximum electric potential gradient is located between the two electrodes (Fig. 3d), and the intensive current density is located in the slag pool region sandwiched by the two face-to-face electrodes. The maximum current density is close to 1.43e6 A·m^{-2}, which is about 3 times greater than the value of the OE process. The region where Joule heat generation is greater than 20 MW·m^{-3} exhibits a strip shape along the longitudinal section of electrode as shown in Fig. 3(f). The Joule heat generation of the TSCE process is more concentrated and powerful than that of the OE process, while the total Joule heat is less than that of the OE process.

Figure 4 presents the distribution of magnetic flux density and electromagnetic force during the ESR process. The direction of magnetic flux density is clockwise in OE process (Fig. 4a), which obeys the right-hand rule of applied current. The maximum magnetic flux density is about 0.0099 T, and is located on the outer surface near the end of the electrode. The electromagnetic force of the slag zone is inward, and the greatest electromagnetic force is around the end of the electrode as shown in Fig. 4(c). For the TSCE process, magnetic flux flows into the slag edge along the central portion of the two face-to-face electrodes, forming two loops that are symmetric with the Y=0 plane, as seen in Fig. 4(b). The maximum magnetic flux density is between the two face-to-face electrodes, and has a value of approximately 0.0145 T. The flux density is more concentrated at the center of the TSCE system than that

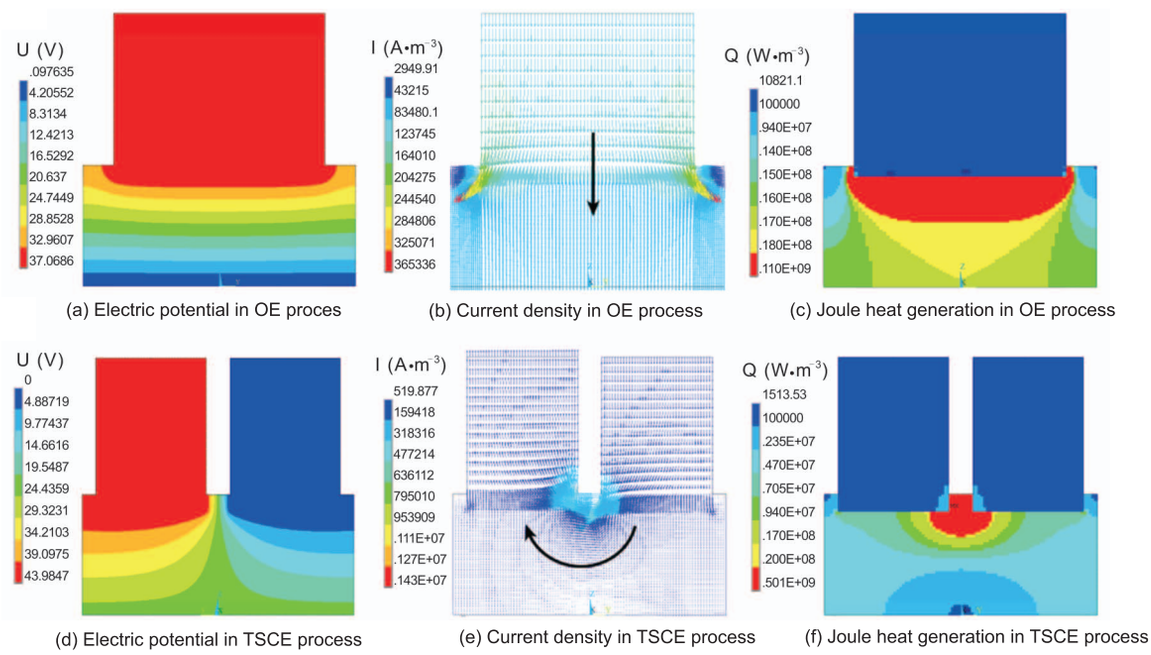

(a) Electric potential in OE proces (b) Current density in OE process (c) Joule heat generation in OE process

(d) Electric potential in TSCE process (e) Current density in TSCE process (f) Joule heat generation in TSCE process

Fig. 3: Distribution of electric potential, current density vector and Joule heat generation in longitudinal section of electrode and slag region in (a), (b) and (c) OE process, and in (d), (e) and (f) TSCE process.

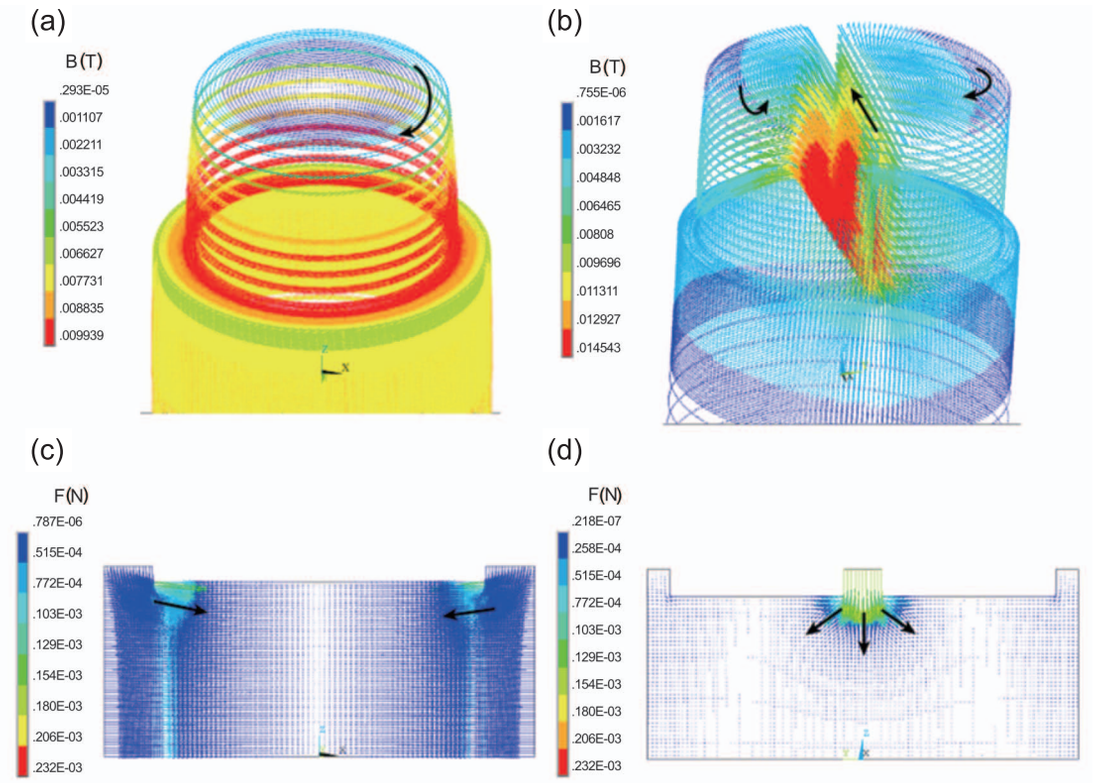

Fig. 4: Magnetic flux density of outer surface of electrode and slag zone with OE process (a) and TSCE process (b), and electromagnetic force on vertical section of slag pool with OE process (c) and TSCE process (d).

of the OE system. The electromagnetic force is outward and downward, pointing from the upper part of slag pool to the slag/metal interface. The greatest electromagnetic force is located in the central portion of the slag, sandwiched by the two face-to-face electrodes (Fig. 4d).

2.2 Flow velocity and temperature fields of slag region

Different Joule heat generation and electromagnetic forces will produce different flow and temperature fields in the slag pool, as shown in Fig. 5. As for the OE process, two large vortices can be found in the lower portion of the slag pool region (Fig. 5a). The liquid slag flows upward into the central portion of the slag pool and down the sidewalls. This means that buoyancy force dominates the hydrodynamic. Due to the strong inward electromagnetic force near the tip of the electrode (Fig. 4c), there are two anti-direction vortices in the upper part of the slag pool. The maximum velocity is about 0.037 $m \cdot s^{-1}$, and is located at the edge of the slag pool region close to the slag/metal interface. The flow characteristics could result in a special temperature distribution in the slag pool as shown in Fig. 5(b). The high temperature zone is below the electrode. The temperature is as high as 1,995 K, and drops rapidly at the slag/metal interface and slag/mold interface.

For the TSCE process, two big vortices form in the upper central portion of the slag region under the strong action of downward electromagnetic force, as shown in Fig. 5(c). Seen from the other direction, the molten slag flows downward and inward from the sidewall to the center, forming two small vortices at the bottom (Fig. 5e). Away from this region, a vortex forms under each electrode. The maximum flow rate is 0.18 $m \cdot s^{-1}$, which is almost five times as great as that of the OE process. The high temperature zone is located in the middle of two electrodes as shown in Fig. 5(d) and Fig. 5(f). The highest temperature is 1,950 K, which is 45 K lower than that of the OE process. Due to the high flow rate, the temperature field distribution of the slag pool of the TSEC process is more uniform than that of the OE process.

2.3 Temperature fields of ESR ingot and experimental verification

Figure 6 shows the temperature distribution of the OE ingot and the TSCE ingot when the ESR process reaches a steady state. It shows that the volume of the OE ingot at a temperature higher than 1,513 K (solidus of M2 alloy) is greater than that of the TSCE ingot. This is because the higher temperature of the OE slag pool could transfer more heat energy to the metal pool. Cooling rate during solidification of the ingot can be expressed as the following form:

$$\dot{T} = G \times R = \frac{T_L - T_S}{\Delta X} \times R \tag{10}$$

where $\dot{T}$ is the the average cooling rate during solidification of the ingot ($K \cdot s^{-1}$). G is the temperature gradient ($K \cdot m^{-1}$). R is the solidification rate ($m \cdot K^{-1}$), which can be simplified to the remelting rate in the steady state. T_L and T_S are respectively the solidus and liquidus (K). ΔX is the width of the mushy

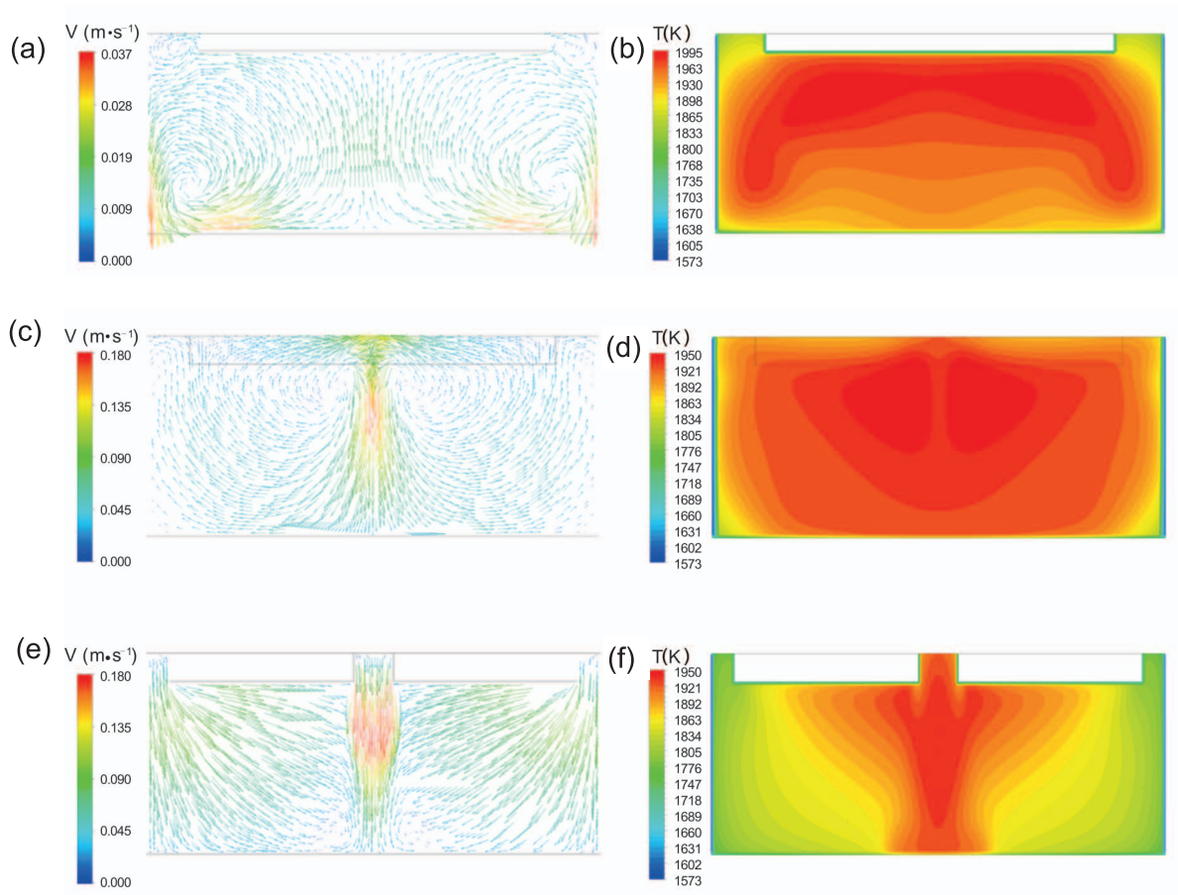

Fig. 5: Flow field (a), (c) and (e) and temperature field (b), (d) and (f) in the longitudinal section of slag pool. (a) and (b) are obtained through OE process, others are through TSCE process. (c) and (d) are central section parallel to the rectangular section of electrodes, and (e) and (f) are central section perpendicular to (c) and (d).

region along the axial direction of the ingot (m). At the center of the ingot, the ΔX of OE ingot is slightly larger than that of TSCE ingot, as shown in Fig. 6. Thus, the G of OE ingot is lower according to equation (10). Since the R (or remelting rate) of the two ingots are the same, the $\dot{T}$ of the OE ingot is less than that of the TSCE ingot. At the periphery of the ingot, there appears to be little difference in the cooling rate of the two ingots. Since the ΔX of the two ingots is narrow, a larger $\dot{T}$ can be obtained at the periphery.

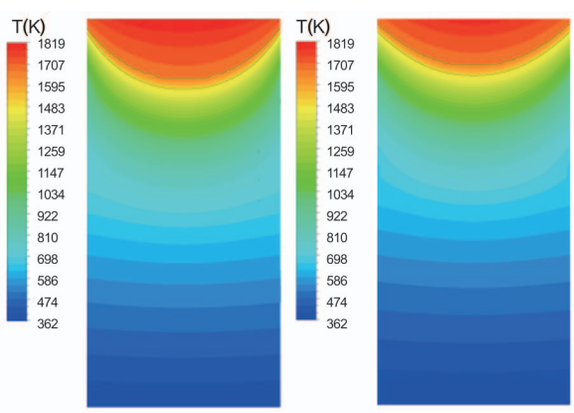

Fig. 6: Temperature distribution of longitudinal section of M2 ingot remelted by OE process (a) and TSCE process (b) (The two green curves stand for liquidus and solidus with a mushy area between them.)

By detecting the shape of the metal pool of ingot after the ESR experiment, the calculated temperature field of the ingot can be indirectly verified, as shown in Fig. 7. The solid brick red curve is obtained from experiment. The black short-dotted curve and the red dotted curve are respectively the equal solidus and equal liquidus from calculation. For the OE process of Fig. 7(a), the metal pool is almost V-shaped, and the pool depth is up to about 160 mm by experiment. The shape of the molten pool is not strictly symmetrical due to the unstable remelting process. It is a symmetrical V-shape with a depth of approximately 150 mm by calculation. The measured curve is mainly located in the calculated mushy zone. For the TSCE process of Fig. 7(b), the depth of V-shaped metal pool is experimentally approximately 120 mm. These experimental curves fall well into the calculated zone, which shows a good match. Furthermore, it is apparent that the metal pool depth of the OE ingot is about 40 mm deeper than the depth of the TSCE ingot.

2.4 Microstructure comparison

Figure 8 shows the eutectic colonies at the center and the periphery of OE ingot and TSCE ingot. For OE ingot, eutectic

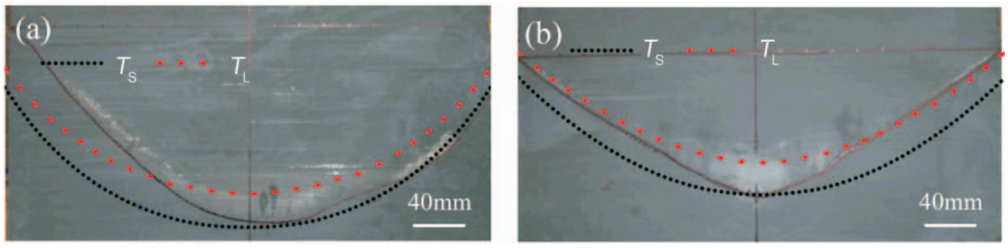

Fig. 7: Metal pool shapes in longitudinal sections of the ESR ingots with the OE process (a) and TSCE process (b) (Brick-red solid curve represents the shape of metal pool by experiment. Black short dash-dotted curve and red dotted curve represents solidus and liquidus by numerical simulation, respectively)

colonies at the center are between 100–400 μm in length as shown in Fig. 8(a). Some equiaxed dendrites nucleate and grow up, eventually forming colonies that are more uneven. Whereas, the directional growth tendency is clear in TSCE ingot of Fig. 8(c). Columnar dendrites can be easily found at the periphery of two ingots in Fig. 8(b) and Fig. 8(d). The colony length of each ingot is between 50–200 μm, which is finer and more uniform than that of the center.

Kurz[18] proposed that the ratio of temperature gradient (G) and growth rate (V) largely determines the growth morphology. The G at the center of OE ingot is lower than that of TSCE ingot. The growth rate (V) at the center of each ingot is equal, because the growth rate (V) could be considered as the solidification rate (R). Therefore, the G/V ratio of TSCE ingot is higher than that of OE ingot, so the TSCE ingot has a strong tendency toward columnar dendrites during solidification. Since the G/V ratio at the edge is much higher than that at the center, finer columnar dendrites can be easily obtained at the edges of two ingots. The electrode configuration seems to have little effect on the size of eutectic colonies around the edge of the ingot.

The morphologies of eutectic carbides of OE ingot and TSCE ingot are compared in Fig. 9. Lamellar M_2C carbides with light gray color and blocky MC carbides with dark gray color could be found in the two ingots. In addition, due to the high temperature annealing, some tiny secondary carbides precipitate from the matrix. At the center of the ingot, the width of M_2C carbides of OE process is as thick as 8 μm, as shown in Fig. 9(a), while the width of TSCE process is less than 4 μm, as shown in Fig. 9(c). M_2C carbides at the edge of two ingots have a width of 1–3 μm [Fig. 9(b) and Fig. 9(d)], which are shorter and thinner than those at the center. The

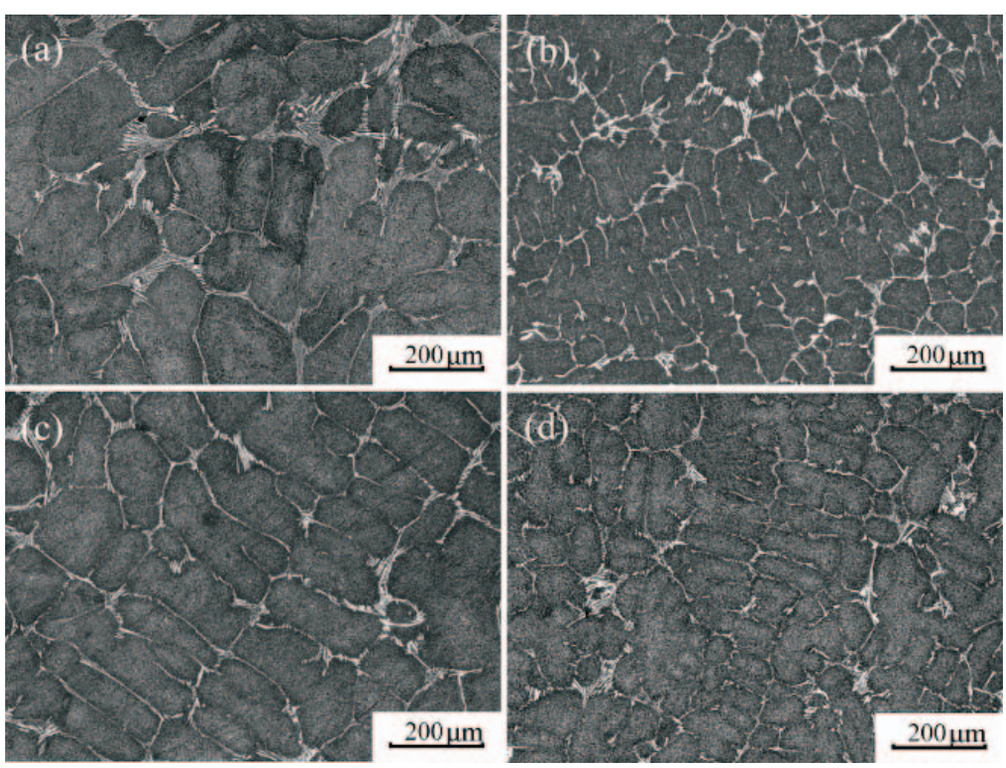

Fig. 8: Eutectic colonies in (a) and (b) OE ingot, and (c) and (d) TSCE ingot. (a) and (c) are located at the center, and (b) and (d) are located at the periphery.

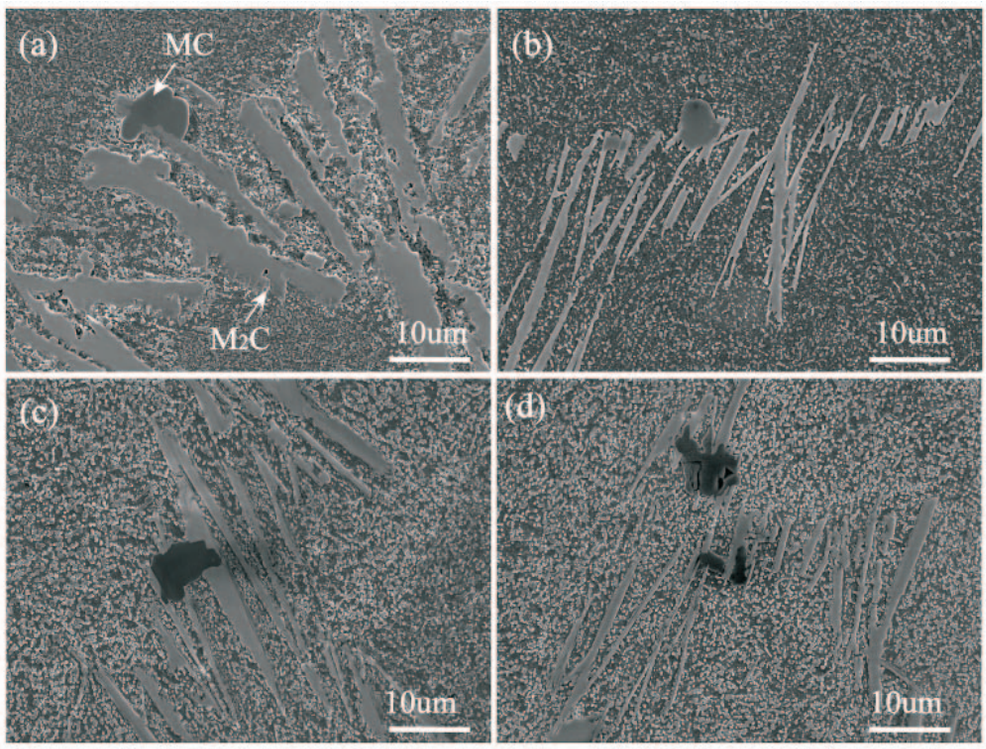

Fig. 9: Morphologies of eutectic carbides in (a) and (b) OE ingot, and (c) and (d) TSCE ingot. (a) and (c) are located at the center, and (b) and (d) are located at the periphery.

scale of eutectic carbide is controlled by the cooling rate. Due to the lowest cooling rate at the OE ingot center as discussed in section 2.3, eutectic carbide can grow for a sufficient time during solidification, and form thicker lamellae. Moreover, these large-sized eutectic carbides require longer time and higher temperatures for heat treatment decomposition. The average length of MC is up to 10 μm at the center of the ingot (Figs. 9a and c), while it decreases to 5–7 μm around the edge (Figs. 9b and d). There is almost no difference in the shape and size of MC carbides for the two ingots. The volume fraction of eutectic carbides at the center of the OE ingot is about 11.2%, while it is close to 6.9% around the edge of the same ingot. Generally, the volume fraction of the OE ingot is nearly 1% higher than that of the TSCE ingot along the radial direction. This would lead to a lower content of alloying elements in the matrix of OE ingot, which is detrimental to the hardness of the final microstructure. In contrast, the TSCE ingot has more uniform distribution of M_2C lamellae and a suitable carbide volume fraction, thus exhibiting better casting quality.

To melt an HSS ingot with a diameter of 400 mm at the same melting rate, the electrical energy consumption of OE process is about 344.1 kW, whereas TSCE process consumes about 33.5% less than that of the OE process. For the TSCE process, the heat generation zone is concentrated and powerful, as calculated in Fig. 3(f), which will provide the strong slag pool flow (Figs. 5c and e) and make the slag pool temperature more uniform and lower (Figs. 5d and f). It will result in less heat energy supply for the TSCE ingot and form a shallower metal pool shape in the ingot (Fig. 7b). Li[19] and Zhan[20] proposed that a shallow and flat molten metal pool obtained under controlled directional solidification of ESR technology can reduce the level of segregation and can modify carbides. Therefore, when compared with the microstructure of the OE ingot, the dendritic structure of the TSCE ingot is more uniform (Fig. 8), and carbides lamellae are thinner, and their volume fraction is lowered (Fig. 9).

3 Conclusions

In order to find a better electroslag remelting (ESR) process for high-speed steel (HSS) ingots, two electrode configuration modes, namely one electrode (OE) and two series-connected electrodes (TSCE), were investigated by finite element simulation and experiment. The principal findings are summarized as follows:

(1) The flow field and temperature field of the ESR system were simulated. For the OE process, two big vortices appear in the lower part of slag pool region with a maximum velocity near the sidewall and a value of approximately 0.037 $m \cdot s^{-1}$. For TSCE process, two vortices are located in the upper part of the slag pool, and the maximum flow velocity is almost 4 times greater than that of OE process. The highest temperature of slag pool of TSCE process is 1,950 K, which is 45 K lower than the temperature of OE process.

(2) The metal pool of OE ingot is V-shaped with an experimental depth of about 160 mm, while the depth of TSCE ingot is nearly 40 mm shallower than that of the OE ingot. Experimental metal pool curves fall well into the calculated

mushy zone, showing a good match.

(3) At the center, coarse equiaxed dendrites are formed in the OE ingot, while more uniform columnar dendrites appear in the TSCE ingot. The width of M_2C carbides of the OE ingot is up to 8 μm, while the width is less than 4 μm in the TSCE ingot. At the periphery, columnar dendrites of the two ingots have almost no difference, and so do the eutectic carbides. The volume fraction of eutectic carbides along the radial direction of OE ingot is about 1% higher than that of the TSCE ingot.

(4) To remelt an HSS ingot with a diameter of 400 mm, the TSCE process is not only more efficient and energy saving, but also achieves a more uniform distribution of carbides in the ingot.

References

[1] Karagöz S, Fischmeister H F. Cutting performance and microstructure of high speed steels: contributions of matrix strengthening and undissolved carbides. Metallurgical & Materials Transactions A, 1998, 29(1): 205–216.
[2] Boccalini M, Goldenstein H. Solidification of high speed steels. Metallurgical Reviews, 2001, 46(2): 92–115.
[3] Campbell J. Sixty years of casting research. Metallurgical & Materials Transactions A, 2015, 46(11): 4848–4853.
[4] Fezi K, Yanke J, Krane M J M. Macrosegregation during electroslag remelting of alloy 625. Metallurgical & Materials Transactions B, 2015, 46(2): 766–779.
[5] Giesselmann N, Rückert A, Eickhoff M, et al. Coupling of multiple numerical models to simulate electroslag remelting process for alloy 718. Transactions of the Iron & Steel Institute of Japan, 2015, 55(7): 1408–1415.
[6] Jeffrey Y, Kyle F, Trice R, et al. Simulation of slag-skin formation in electroslag remelting using a volume-of-fluid method. Numerical Heat Transfer, 2015, 67(3): 268–292.
[7] Li Baokuan, Wang Bo, Tsukihashi F. Modeling of electromagnetic field and liquid metal pool shape in an electroslag remelting process with two series-connected electrodes. Metallurgical & Materials Transactions B, 2014, 45(3): 1122–1132.
[8] Liu Xihai, Wang Junqing, Jia Weiguo, et al. Simulation of electro-slag re-melting process of 120t large ingot for nuclear power station and its application. China Foundry, 2011, 8(4): 413–417.
[9] Dong Yanwu, Jiang Zhouhua, Liu Hui, et al. Simulation of multi-electrode ESR process for manufacturing large ingot. ISIJ International, 2012, 52(12): 2226–2234.
[10] Liu F B, Jiang Z H, Li H B, et al. Mathematical modelling of electroslag remelting P91 hollow ingots process with multi-electrodes. Ironmaking & Steelmaking, 2014, 41(10): 791–800.
[11] Ren N, Li BK, Li LM, et al. Numerical investigation on the fluid flow and heat transfer in electroslag remelting furnace with triple-electrode. Ironmaking & Steelmaking, 2016(1): 1–10.
[12] Hernandez-Morales B, Mitchell A. Review of mathematical models of fluid flow, heat transfer, and mass transfer in electroslag remelting process. Ironmaking & Steelmaking, 1999, 26(6):423–438.
[13] Dong Yanwu, Hou Zhiwen, Jiang Zhouhua, et al. Study of a single-power two-circuit ESR process with current-carrying mold: mathematical simulation of the process and experimental verification. Metallurgical & Materials Transactions B, 2018, 49(1): 349–360.
[14] Kharicha A, Karimi-Sibaki E, Wu Menghuai, et al. Review on modeling and simulation of electroslag remelting. Steel Research International, 2018, 89: 1–20.
[15] Wang Qiang, Li Baokuan. Numerical Investigation on the effect of slag thickness on metal pool profile in electroslag remelting process. ISIJ International, 2016, 56(2): 282–287.
[16] Zhou Xuefeng, Fang Feng, Jiang Jianjing. Solidification microstructure of M2 high speed steel by different casting technologies. China Foundry, 2011, 8(3): 290–294.
[17] Fischmeister H F, Riedl R, Karagöz S. Solidification of high-speed tool steels. Metallurgical Transactions A, 1989, 20(10): 2133–2148.
[18] Kurz W. Fisher D J. Fundamentals of solidification. Switzerland: Trans Tech Publications Ltd, 1998: 87–89.
[19] Li Fulin, Fu Rui, Feng Di, et al. Microstructure and segregation behavior of Rene88DT alloy prepared by ESR-CDS. Rare Metal Materials & Engineering, 2016, 45(6): 1437–1442.
[20] Zhan Lichun, Chi Hongxiao, Ma Dangshen, et al. The as-cast microstructure of ESR-CDS M2 high speed steel. Material Engineering, 2013, 24(7): 29–34. (In Chinese)

This work was financially surpported by the Foundation of Hebei Provincial Department of Education,China (Grant No. QN2018034 and QN2017051).